PAPER

Axial and equatorial ligand effects on biomimetic cysteine dioxygenase model complexes†

Luis E. Gonzalez-Ovalle,[a] Matthew G. Quesne,[a] Devesh Kumar,*[b] David P. Goldberg*[c] and Sam P. de Visser*[a]

Density functional theory (DFT) calculations are presented on biomimetic model complexes of cysteine dioxygenase and focus on the effect of axial and equatorial ligand placement. Recent studies by one of us [Y. M. Badiei, M. A. Siegler and D. P. Goldberg, *J. Am. Chem. Soc.* 2011, **133**, 1274] gave evidence of a nonheme iron biomimetic model of cysteine dioxygenase using an *i*-propyl-bis(imino)pyridine, equatorial tridentate ligand. Addition of thiophenol, an anion – either chloride or triflate – and molecular oxygen, led to several possible stereoisomers of this cysteine dioxygenase biomimetic complex. Moreover, large differences in reactivity using chloride as compared to triflate as the binding anion were observed. Here we present a series of DFT calculations on the origin of these reactivity differences and show that it is caused by the preference of coordination site of anion *versus* thiophenol binding to the chemical system. Thus, stereochemical interactions of triflate and the bulky iso-propyl substituents of the ligand prevent binding of thiophenol in the *trans* position using triflate. By contrast, smaller anions, such as chloride, can bind in either *cis* or *trans* ligand positions and give isomers with similar stability. Our calculations help to explain the observance of thiophenol dioxygenation by this biomimetic system and gives details of the reactivity differences of ligated chloride *versus* triflate.

Introduction

Nonheme iron enzymes are versatile oxidants that catalyze a range of vital processes for human health, and are involved in repair mechanisms, biosynthesis as well as biodegradation of compounds. Generally, they use molecular oxygen on an iron center and transfer either one or both oxygen atoms of molecular oxygen to a substrate, whereby a monoxygenation, dioxygenation or dehydrogenation type of reaction occurs. Nature has developed a large arsenal of these nonheme iron enzymes with various differences in ligand orientation and binding as well as functional properties.[1] Studies on nonheme iron containing enzymes and synthetic analogues (biomimetic compounds) are important for the understanding of biochemical reaction mechanisms but also for industrial (biotechnological) applications.

An extensively studied class of nonheme iron enzymes is the α-ketoglutarate dependent dioxygenases, which anchor the metal *via* a facial 2-His-1-Asp ligand orientation to the protein.[2] These enzymes catalyze the biosynthesis of several antibiotics in bacteria; including vancomycin, fosfomycin and carbapenem.[3] In addition, these enzymes have been implicated with DNA and RNA repair mechanisms.[4] A structurally similar enzyme to the α-ketoglutarate dependent dioxygenases is the human enzyme cysteine dioxygenase (CDO), which is involved in the detoxification and metabolism of cysteine in the body.[5] It catalyzes the first step in the biodegradation of cysteine and converts the substrate to cysteine sulfinic acid. This is a unique reaction and of interest to the biotechnology industry for the catalytic dioxygenation of sulphides.

CDO contains an unusual ligand system where the metal is bound to three histidine ligands of the protein *via* a 3-His facial ligand orientation, but compared to the α-ketoglutarate dependent dioxygenases lacks the carboxylate ligand and the 2-His/1-Asp motif. Current evidence suggests the substrate cysteinate binds the metal in a bidentate fashion through the thiolate and amine groups and is locked in hydrogen bonding interactions *via* several nearby polar amino acids. Fig. 1 displays the active site of substrate bound CDO as taken from the 2IC1 protein databank (pdb) structure.[6] Similar to the nonheme iron dioxygenases, the protein binds the metal in a facial orientation and the ligand position *trans* to His86 is vacant and is reserved for molecular oxygen. In recent years a number of spectroscopic and kinetic

[a] Manchester Interdisciplinary Biocenter and School of Chemical Engineering and Analytical Science, The University of Manchester, 131 Princess Street, Manchester M1 7DN, UK. E-mail: sam.devisser@manchester.ac.uk; Fax: +44 (0)161306 5201
*[b] Department of Applied Physics, School of Physical Sciences, Babasaheb, Bhimrao Ambedkar University, Vidya Vihar, Rae Bareilly Road, Lucknow 226-025, India. E-mail: dkclcre@yahoo.com*
*[c] Department of Chemistry, The Johns Hopkins University, 3400 N. Charles Street, Baltimore, Maryland 21218, USA. E-mail:dpg@jhu.edu*
†Electronic supplementary information (ESI) available. See DOI: 10.1039/c2ob25406a

This journal is © The Royal Society of Chemistry 2012

Org. Biomol. Chem., 2012, **10**, 5401–5409 | 5401
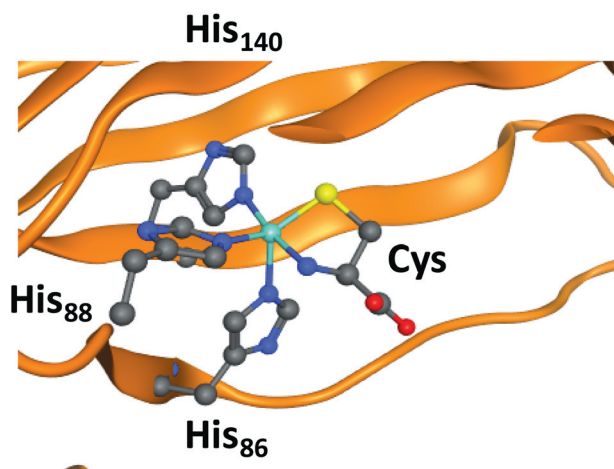
Fig. 1 Extract of the active site of CDO as taken from the 2IC1 pdb file.[6] Amino acids are labelled as in the pdb.
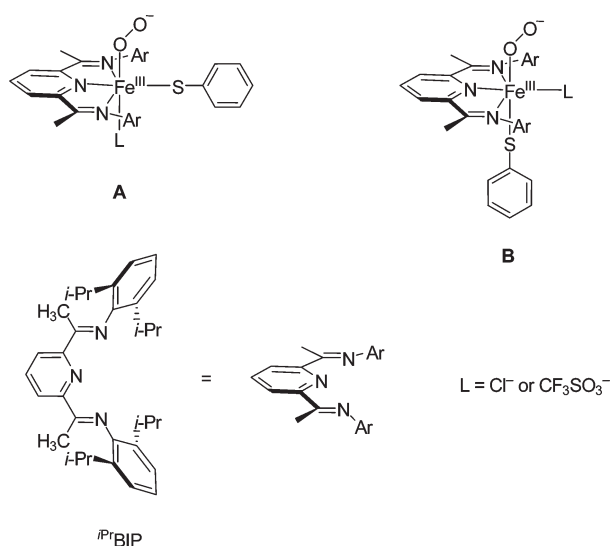
Scheme 1 Models investigated in this study.

studies have provided important insight on the catalytic mechanism of CDO, but there is little knowledge of oxygen bound intermediates.[7] A series of computational studies in our groups have given insight into the CDO ligand system and its mechanism of substrate activation.[8] These studies showed that replacing the 3-His ligand system of CDO by a 2-His-1-Asp ligand system disrupts the dioxygenation process of cysteine and, in particular, leads to weakening of the Fe–S bond. It appears, therefore, that the 3-His ligand system is essential for optimal dioxygenation of cysteine.

In biomimetic chemistry, active site analogues are created with the aim to understand the basic features of enzyme active site structures and reactivity.[1c,d,9] Recently, a few biomimetic models of CDO enzymes were published and spectroscopically characterized.[10–12] One of these contains an Fe(II)(^{iPr}BIP) complex (^{iPr}BIP = iso-propyl-bis(imino)pyridine), Scheme 1.[11] Studies focused on the relative orientation of thiophenol and dioxygen on the metal center. Thus, the ^{iPr}BIP ligand occupies three ligand positions of the metal in the same plane. Dioxygen

will occupy the ligand position *cis* with respect to the three nitrogen atoms of the ^{iPr}BIP ligand. The remaining two ligand positions are occupied by thiophenolate (SPh$^-$) and an anion, which is either Cl$^-$ or CF$_3$SO$_3^-$. Consequently, these complexes have two possible stereoisomers (Scheme 1) for the Fe(III)-superoxo complex, *i.e.* [Fe^{III}O$_2$(^{iPr}BIP)(SPh)(L)] with L = Cl$^-$ or CF$_3$SO$_3^-$ (OTf$^-$), which are designated with **A** and **B** in Scheme 1, respectively. It also should be noted that in contrast to the facial triad of histidine ligands in CDO enzymes, the ^{iPr}BIP ligand coordinates in one plane thereby leaving the axial ligand position vacant for either substrate or an anion. The previous experimental studies revealed dramatic differences in reactivity that were induced by changing the ligand L from Cl$^-$ to CF$_3$SO$_3^-$, whereby the chloride ligated complex gave disulfide products, whereas the triflate ligated system reacted with O$_2$ to give an *S*-oxygenated sulfonato product.[11] These differences were assigned to axial *versus* equatorial ligand effects on the iron complex, however, direct evidence for this mechanistic hypothesis was lacking. To gain insight into this matter we performed a density functional theory (DFT) study, and the results are present here.

The effect of axial and equatorial ligands on heme and nonheme iron oxidants is well documented. Thus, heme monooxygenases such as the cytochromes P450 contain an iron-heme active center where the heme is linked to the protein *via* an axial cysteinate ligand.[13] By contrast, heme peroxidases have an axially ligated histidine group, which has been proposed to be a key reason for their differences in catalytic function.[14] These studies proposed the cysteinate to act with a "push"-effect and the push/pull-effect of the axial ligand is thought to contribute to the reactivity differences of P450s *vis-à-vis* peroxidases. Indeed, a series of density functional theory (DFT) calculations confirmed that peroxidase models reacted with much higher barriers in aliphatic hydroxylation and epoxidation reactions using the same substrate.[15] Moreover, the differences between an axially ligated cysteinate *versus* histidine were explained as originating from the charge of the axial ligand and the molecular orbital interactions between metal and ligand.[16]

In biomimetic models, the effect of the axial ligand on spectroscopic properties (*trans*-influence) as well as on reactivity patterns (*trans*-effect) was demonstrated by Gross and co-workers[17] using studies of styrene epoxidation by a range of iron(IV)-oxo porphyrin cation radical systems. Subsequent studies of Nam *et al*[18] showed differences in oxidative properties of iron(IV)-oxo oxidants with chloride *trans* to the oxo group as compared to those with acetonitrile, leading to reactivity differences of those oxidants with *cis versus trans* olefins, the regioselectivity of aliphatic over aromatic hydroxylation, as well as epoxidation *versus* hydroxylation processes. Further studies also revealed axial ligand effects on the reactivity and spectroscopic parameters of a selection of nonheme iron complexes,[19] including a series of thiolate-ligated nonheme iron model complexes by one of us.[20] Recent, combined experimental and computational studies in our groups on the reactivity of manganese(V)-oxo embedded in a corrolazine ligand system identified a pronounced axial ligand effect on the rate constant of hydrogen atom abstraction from C–H substrates (*e.g.* dihydroanthracene) as a function of the axial ligand.[21] By contrast, very little is known of the ligand effect of iron(III)-superoxo complexes,

which we will address in this work. The computational study presented here provides insight into the equatorial and axial ligand effect of the CDO biomimetic model displayed in Scheme 1.
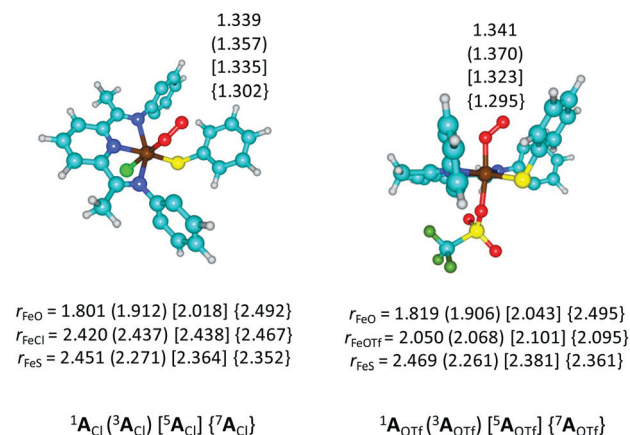
Methods

The studies presented in this work use density functional theory methods as implemented in the *Gaussian*-03 program package.[22] Following previous experience in the field,[23] we initially used the unrestricted hybrid density functional method UB3LYP[24] in combination with a double-ζ quality LANL2DZ basis set on iron that includes a core potential and 6-31G on the rest of the atoms,[25] basis set BS1. We performed a full geometry optimization (without constraints) followed by an analytical frequency calculation. All structures were confirmed as local minima and had no imaginary frequencies. Subsequent geometry optimization and frequency calculations were done with a triple-ζ quality basis set: BS2 represents a triple-ζ LACV3P+ basis set on iron and 6-311+G* on the rest of the atoms and BS3 is 6-311+G* on all atoms. It should be noted that very little differences in energy and optimized geometries are obtained between UB3LYP/BS2//UB3LYP/BS1 calculations as compared to those found for UB3LYP/BS2 optimizations, therefore, we will focus on only the latter results.[26] All calculations were done for the lowest lying singlet, triplet, quintet and septet spin states. To test the effect of the environment on the ordering and relative energies of the various spin states, we did single point calculations using the polarized continuum model (PCM) with a dielectric constant of $\varepsilon = 35.7$ mimicking an acetonitrile solution at UB3LYP/BS2.

To confirm the obtained spin state ordering and relative energies we did a further set of calculations using dispersion corrected density functional theory (B3LYP-D).[27] We reoptimized $^{3,5,7}\mathbf{A_L}$ and $^{3,5,7}\mathbf{B_L}$ (L = Cl⁻/OTf⁻) at B3LYP-D/BS1 level of theory followed by a single point calculation at B3LYP-D/BS2 level of theory. The methods used in this work are well tested and benchmarked. For example, they have reproduced experimental free energies of activation of oxygen atom transfer processes within about 3 kcal mol⁻¹.[28]

Results and discussion

We started our investigation with a series of calculations on $^{1,3,5,7}\mathbf{A_L}$ (L = Cl⁻ and OTf⁻) and the optimized geometries are given in Fig. 2, whereas the relative energies of the individual spin states are given in Table 1. The method has very little effect on the spin state ordering, which is virtually constant for all models described in this work. Generally, the septet and triplet spin states are destabilized with dispersion corrections included. Nevertheless, the results appear to give close lying quintet and septet spin iron(III)-superoxo intermediates.

We, generally, find minor structural differences between geometries optimized at UB3LYP/BS1 (Fig. 2) and UB3LYP-D/BS1 (Fig. S3, ESI†) level of theory for most key intermediates. In both cases the quintet and septet spin states are degenerate, whereby the septet state is the lowest by a few kcal mol⁻¹ at B3LYP but dispersion corrections make the quintet slightly

r_{FeO} = 1.801 (1.912) [2.018] {2.492} r_{FeO} = 1.819 (1.906) [2.043] {2.495}
r_{FeCl} = 2.420 (2.437) [2.438] {2.467} r_{FeOTf} = 2.050 (2.068) [2.101] {2.095}
r_{FeS} = 2.451 (2.271) [2.364] {2.352} r_{FeS} = 2.469 (2.261) [2.381] {2.361}

$^{1}\mathbf{A_{Cl}}$ ($^{3}\mathbf{A_{Cl}}$) [$^{5}\mathbf{A_{Cl}}$] {$^{7}\mathbf{A_{Cl}}$} $^{1}\mathbf{A_{OTf}}$ ($^{3}\mathbf{A_{OTf}}$) [$^{5}\mathbf{A_{OTf}}$] {$^{7}\mathbf{A_{OTf}}$}

Fig. 2 Optimized geometries of $^{1,3,5,7}\mathbf{A_{Cl}}$ (left-hand-side) and $^{1,3,5,7}\mathbf{A_{OTf}}$ (right-hand-side) with bond lengths in angstroms. Isopropyl groups have been hidden.

Table 1 Spin state ordering and relative energies of $^{1,3,5,7}\mathbf{A_L}$ and $^{1,3,5,7}\mathbf{B_L}$ (L = Cl⁻/OTf⁻) as obtained using different methods and techniques[a]

	B3LYP/ BS1	B3LYP/ BS2	B3LYP + E_{solv}/BS2	B3LYP-D/ BS1	B3LYP-D/ BS2
$^{1}\mathbf{A_{Cl}}$	26.05	25.55	32.00		
$^{3}\mathbf{A_{Cl}}$	12.56	11.73	16.13	27.16	39.19
$^{5}\mathbf{A_{Cl}}$	0.00	0.00	0.00	0.00	0.00
$^{7}\mathbf{A_{Cl}}$	−0.27	−8.11	−2.66	−0.11	0.21
$^{1}\mathbf{A_{OTf}}$	26.16	31.84	32.36		
$^{3}\mathbf{A_{OTf}}$	5.94	11.47	11.31	18.50	31.27
$^{5}\mathbf{A_{OTf}}$	0.00	0.00	0.00	0.00	0.00
$^{7}\mathbf{A_{OTf}}$	−0.55	−1.91	−2.41	0.65	1.46
$^{1}\mathbf{B_{Cl}}$	29.73	28.18	32.72		
$^{3}\mathbf{B_{Cl}}$	10.72	9.42	15.49	24.58	35.71
$^{5}\mathbf{B_{Cl}}$	2.62	1.16	7.46	20.96	12.15
$^{7}\mathbf{B_{Cl}}$	−7.56	−18.40	−11.75	−7.55	−9.21
$^{1}\mathbf{B_{OTf}}$	37.05	41.67	37.51		
$^{3}\mathbf{B_{OTf}}$	19.70	31.24	26.60	61.03	75.68
$^{5}\mathbf{B_{OTf}}$	15.03	23.73	20.15	43.55	39.19
$^{7}\mathbf{B_{OTf}}$	5.09	9.16	5.03	27.42	33.90

[a] All data are in kcal mol⁻¹ and include zero-point corrections. E_{solv} stands for solvent corrected energy.

lower in energy. The triplet (singlet) spin states are well higher in energy by 19.8 (33.7) kcal mol⁻¹ for $\mathbf{A_{Cl}}$ and 13.4 (33.8) kcal mol⁻¹ for $\mathbf{A_{OTf}}$, and we conclude that these two spin states are unlikely to play a role of importance in the reaction mechanism. With dispersion corrections included, these spin states are further raised in energy. Recent spectroscopic studies on a synthetically generated iron(III)-superoxo CDO intermediate found evidence of a septet spin ground state.[29] Although these enzymatic CDO studies contradict other nonheme iron(III)-superoxo work,[30] where quintet spin ground states are found, the work does support the calculations presented here. Consequently, the availability of a low-lying septet spin state may be inherent to the ligand system of CDO enzymes and their biomimetic model complexes. However, these results do not require that the reactivity take place on the septet spin state surface, as will be seen later.

Optimized geometries are in line with previous computational studies on Fe(III)-superoxo complexes that typically find O–O
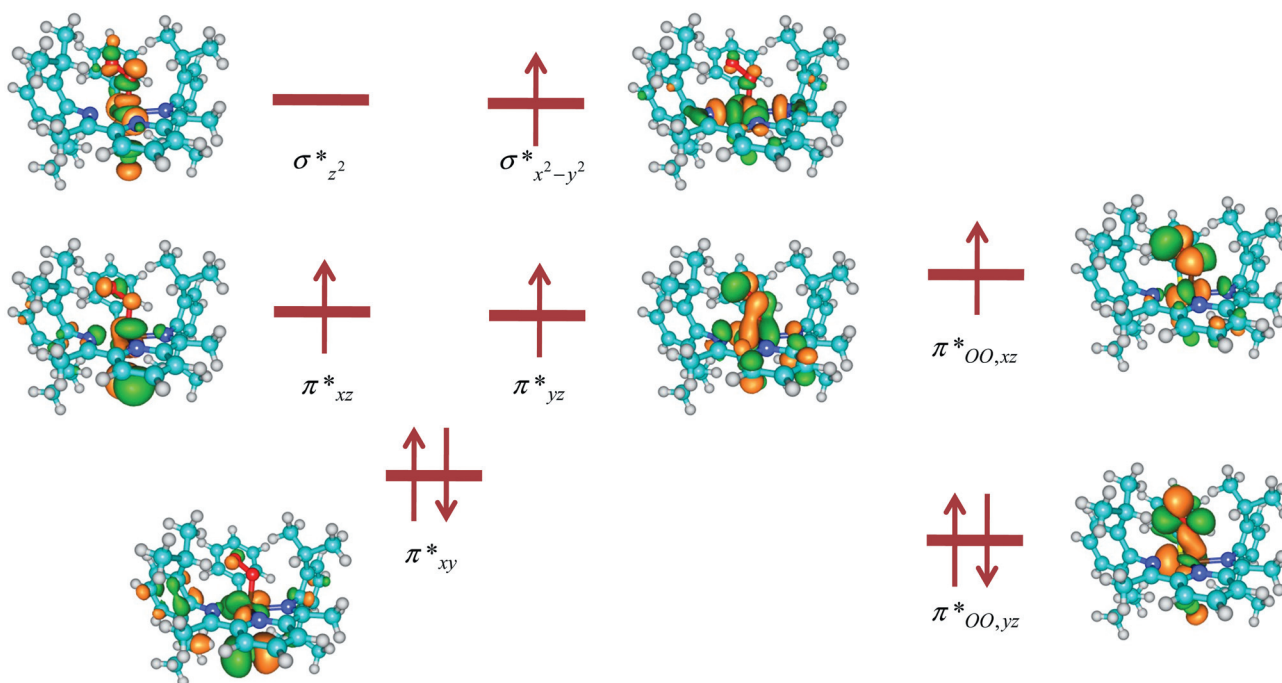
Fig. 3 High-lying occupied and low-lying virtual orbitals of $^5A_{Cl}$.

distances in the range of 1.295–1.370 Å.[31] The Fe–Cl distance is in a narrow range from 2.420–2.467 Å, which is in good agreement with previous studies of iron(IV)-oxo porphyrin cation radical systems that also had an axially ligated Cl$^-$ anion.[32] There is some fluctuation in the Fe–S bond length between the four different spin states, however, this follows from the molecular orbital occupations, *vide infra*.
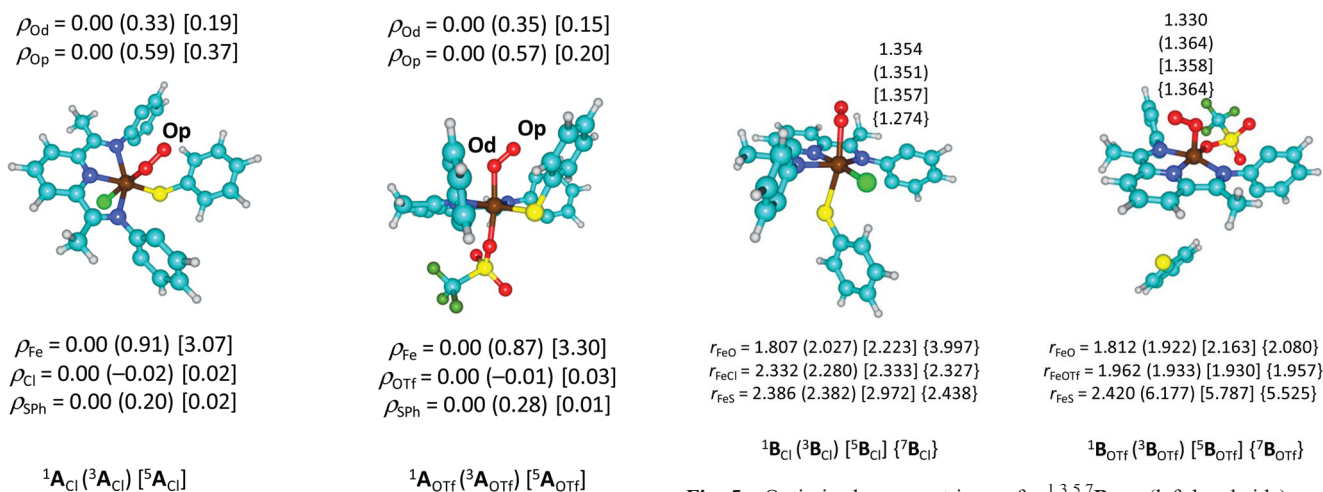
To understand these spin state energetics and the differences between models A_{Cl} and A_{OTf}, consider in Fig. 3 the high-lying occupied and virtual orbitals for both systems as taken from the quintet spin calculations. The metal-type orbitals originate from a linear combination of the 3d atomic orbitals on iron with ligand based orbitals. The lowest lying orbital is the π^*_{xy} orbital that is in the plane of the ^{iPr}BIP ligand. A bit higher in energy are the π^*_{xz} and π^*_{yz} orbitals; the former is in the plane of the Fe–O–O group and interacts with a π-orbital on the axial ligand, while the π^*_{yz} orbital interacts with both the axial ligand and the proximal oxygen atom. Higher in energy are two σ* orbitals: one for the antibonding interaction of the axial ligand and the proximal oxygen atom with the iron ($\sigma^*_{z^2}$) and the second for the antibonding interactions of the metal with the BIP and phenylthiolate ligands ($\sigma^*_{x^2-y^2}$). Two antibonding orbitals along the superoxo bond are also depicted in Fig. 3 ($\pi^*_{OO,yz}$ and $\pi^*_{OO,xz}$), which are occupied with three electrons. The metal-based orbitals are occupied with five electrons, and the system is characterized as an Fe(III)-superoxo complex with a quintet spin state.

The quintet spin state has orbital occupation $\pi^*_{xy}{}^2$ $\pi^*_{xz}{}^1$ $\pi^*_{yz}{}^1$ $\sigma^*_{x^2-y^2}{}^1$ $\pi^*_{OO,yz}{}^2$ $\pi^*_{OO,xz}{}^1$ and includes the ferromagnetic coupling of the $\pi^*_{OO,xz}$ electron with three metal based unpaired electrons. The lowest lying triplet spin state, by contrast, has $\pi^*_{xy}{}^2$ $\pi^*_{yz}{}^2$ $\pi^*_{xz}{}^1$ $\pi^*_{OO,yz}{}^2$ $\pi^*_{OO,xz}{}^1$ and is distinguished from the quintet spin state by the transfer of one electron from $\sigma^*_{x^2-y^2}$ to π^*_{yz}. This conversion is equivalent to a change from intermediate-spin Fe^{III} to a low-spin Fe^{III} ion. Both of these states,

therefore, can be characterized as Fe(III)-superoxo complexes. The septet and singlet spin states, by contrast, are Fe(II)-dioxygen complexes with orbital occupation $\pi^*_{xy}{}^2$ $\pi^*_{xz}{}^1$ $\pi^*_{yz}{}^1$ $\sigma^*_{x^2-y^2}{}^1$ $\sigma^*_{z^2}{}^1$ $\pi^*_{OO,yz}{}^1$ $\pi^*_{OO,xz}{}^1$ and $\pi^*_{xy}{}^2$ $\pi^*_{xz}{}^2$ $\pi^*_{yz}{}^2$ $\pi^*_{OO,yz}{}^2$, respectively. We made several attempts to swap orbitals for the singlet spin state and calculate a low-spin Fe(III)-superoxo complex but all our calculations converged back to the Fe(II)-dioxygen situation instead. It appears therefore that there is no lower lying low-spin state for these complexes. The orbital occupation is in line with previous experimental and computational studies of six-coordinate iron(III)-superoxo complexes.[30,33,34]

The pentacoordinated iron(II)-^{iPr}BIP(X) reactant complex with X = Cl$^-$ or OTf$^-$ was characterized as a quintet spin state,[11] therefore, dioxygen binding may continue on the quintet spin state surface rather than generating a septet spin iron(II)-dioxygen state. In light of the large geometric differences between the quintet and septet structures, this would imply small spin–orbit coupling between the two states and little equilibration between the two spin states. Our optimized geometries are also in support of the orbital occupations, and, for instance, in the quintet spin state due to single occupation of a $\sigma^*_{x^2-y^2}$ orbital with antibonding character along the Fe–SPh axis, the Fe–S distances are elongated with respect to the triplet spin state, where this orbital is virtual. The same trend is also observed for $^{1,3,5,7}A_{OTf}$. On the other hand, occupation of the $\sigma^*_{z^2}$ orbital in the quintet spin state would have elongated the Fe–O and Fe–axial ligand distances considerably, as observed before.[35] The geometries, therefore, support the assignment of a singly occupied $\sigma^*_{x^2-y^2}$ orbital and virtual $\sigma^*_{z^2}$ orbital in the quintet spin states.

The group spin densities (Fig. 4) give further evidence for the assignment of the orbital occupations discussed above. In the triplet spin state the unpaired spin density on the superoxo group is 0.92 for both $^3A_{Cl}$ and $^3A_{OTf}$, which is coupled to an unpaired electron on the metal; the spin density on iron is 0.91 in $^3A_{Cl}$

$\rho_{Od} = 0.00 \ (0.33) \ [0.19]$
$\rho_{Op} = 0.00 \ (0.59) \ [0.37]$

$\rho_{Fe} = 0.00 \ (0.91) \ [3.07]$
$\rho_{Cl} = 0.00 \ (-0.02) \ [0.02]$
$\rho_{SPh} = 0.00 \ (0.20) \ [0.02]$

$^1\mathbf{A}_{Cl} \ (^3\mathbf{A}_{Cl}) \ [^5\mathbf{A}_{Cl}]$

$\rho_{Od} = 0.00 \ (0.35) \ [0.15]$
$\rho_{Op} = 0.00 \ (0.57) \ [0.20]$

$\rho_{Fe} = 0.00 \ (0.87) \ [3.30]$
$\rho_{OTf} = 0.00 \ (-0.01) \ [0.03]$
$\rho_{SPh} = 0.00 \ (0.28) \ [0.01]$

$^1\mathbf{A}_{OTf} \ (^3\mathbf{A}_{OTf}) \ [^5\mathbf{A}_{OTf}]$

Fig. 4 Group spin densities calculated at UB3LYP/B2//UB3LYP/B1 for $^{1,3,5,7}\mathbf{A}_{Cl}$ (left-hand-side) and $^{1,3,5,7}\mathbf{A}_{OTf}$ (right-hand-side). H-atoms and isopropyl group have been hidden.

1.354
(1.351)
[1.357]
{1.274}

$r_{FeO} = 1.807 \ (2.027) \ [2.223] \ \{3.997\}$
$r_{FeCl} = 2.332 \ (2.280) \ [2.333] \ \{2.327\}$
$r_{FeS} = 2.386 \ (2.382) \ [2.972] \ \{2.438\}$

$^1\mathbf{B}_{Cl} \ (^3\mathbf{B}_{Cl}) \ [^5\mathbf{B}_{Cl}] \ \{^7\mathbf{B}_{Cl}\}$

1.330
(1.364)
[1.358]
{1.364}

$r_{FeO} = 1.812 \ (1.922) \ [2.163] \ \{2.080\}$
$r_{FeOTf} = 1.962 \ (1.933) \ [1.930] \ \{1.957\}$
$r_{FeS} = 2.420 \ (6.177) \ [5.787] \ \{5.525\}$

$^1\mathbf{B}_{OTf} \ (^3\mathbf{B}_{OTf}) \ [^5\mathbf{B}_{OTf}] \ \{^7\mathbf{B}_{OTf}\}$

Fig. 5 Optimized geometries of $^{1,3,5,7}\mathbf{B}_{Cl}$ (left-hand-side) and $^{1,3,5,7}\mathbf{B}_{OTf}$ (right-hand-side) with bond lengths in angstroms. Isopropyl groups have been hidden.

and 0.87 in $^3\mathbf{A}_{OTf}$. These spin densities confirm the single occupation of the π^*_{xz} and $\pi^*_{OO,xz}$ orbitals in these triplet spin states. In the quintet spin states, by contrast, the metal unpaired spin density is increased to 3.07 and 3.30 for $^5\mathbf{A}_{Cl}$ and $^5\mathbf{A}_{OTf}$, respectively. The metal is involved in all four singly occupied molecular orbitals, although the contribution is small in $\pi^*_{OO,xz}$ (Fig. 3). In the quintet spin states there is also significant spin density on the BIP ligand system (0.30 in $^5\mathbf{A}_{Cl}$ and 0.33 in $^5\mathbf{A}_{OTf}$), which further supports the assignment of a singly occupied $\sigma^*_{x^2-y^2}$ orbital.

Subsequently, we investigated the isomers $^{1,3,5,7}\mathbf{B}_{Cl}$ and $^{1,3,5,7}\mathbf{B}_{OTf}$, which have the axial and equatorial ligands swapped as compared to structure $\mathbf{A}_L$ (L = Cl$^-$ or OTf$^-$), Scheme 1, i.e. the thiophenolate is put in the axial position of the iron(III)-superoxo and the anionic ligand (Cl$^-$ or OTf$^-$) is in the equatorial position. Optimized geometries of the lowest lying singlet, triplet, quintet and septet spin state structures are depicted in Fig. 5. Similarly to the results described above on $^{1,3,5,7}\mathbf{A}_{Cl}$, also for $\mathbf{B}_{Cl}$ the septet spin state is the ground state followed by the quintet and triplet spin states, whereas the closed-shell singlet spin state is well higher in energy. Relative energies of the four spin states are: $^7\mathbf{B}_{Cl}$ (0.0 kcal mol^{-1}), $^5\mathbf{B}_{Cl}$ (19.6 kcal mol^{-1}) $^3\mathbf{B}_{Cl}$ (27.8 kcal mol^{-1}) and $^1\mathbf{B}_{Cl}$ (46.6 kcal mol^{-1}). It appears, therefore, that the septet spin state is considerably stabilized over the other three spin states, although the relative energies between $^{1,3,5}\mathbf{A}$ and $^{1,3,5}\mathbf{B}$ are not dramatically different.

Geometrically, there are similarities as well as differences between the structures $^{1,3,5,7}\mathbf{A}_{Cl}$, on the one hand, and $^{1,3,5,7}\mathbf{B}_{Cl}$, on the other hand. First of all in $^7\mathbf{B}_{Cl}$ the oxygen group is not bound to the metal center, whereas in $^7\mathbf{B}_{OTf}$ one ligand (SPh) has split off the metal center. Recent studies of ours[36] showed that it is essential for sulphur oxygenation that dioxygen binds to the metal center prior to the reaction. Consequently, the septet structures are unlikely to be involved in the reaction mechanism for S-oxygenation. Despite the fact that the dioxygen bond length is virtually the same in all complexes, actually the metal–ligand distances show big differences. Thus, the metal–oxygen bond is significantly elongated from 1.912 Å in $^3\mathbf{A}_{Cl}$ to 2.027 Å

in $^3\mathbf{B}_{Cl}$ and from 2.018 Å in $^5\mathbf{A}_{Cl}$ to 2.223 Å in $^5\mathbf{B}_{Cl}$. At the same time elongation of the Fe–S bond occurs from 2.271 Å in $^3\mathbf{A}_{Cl}$ to 2.382 Å in $^3\mathbf{B}_{Cl}$ and from 2.364 Å in $^5\mathbf{A}_{Cl}$ to 2.972 Å in $^5\mathbf{B}_{Cl}$. The latter structure has a very weak thiophenolate bound and with a bond length of that magnitude cannot be considered as a covalent bond.

In the triflate bound isomers ($^{3,5,7}\mathbf{B}_{OTf}$) this situation is even worse and the thiophenolate has dissociated completely from the metal and is optimized with a distance of around 6 Å. Hence, $^{3,5,7}\mathbf{B}_{OTf}$ are pentacoordinate complexes. The reason for this is the considerable steric strain from the di-iso-propylphenyl groups that are attached to the BIP ligand. The group spin densities of these complexes characterize these structures as Fe(II)-superoxo with a nearby thiophenol radical, i.e. an electron transfer from thiophenol to the metal has taken place. This electron transfer fills the π^*_{xz} orbital with a second electron in both the triplet and quintet spin states. A single point calculation in a dielectric constant does not change the spin and charge distributions dramatically and keeps the system in a Fe(II)-superoxo-^{iPr}BIP-(OTf) with a nearby SPh$^\cdot$ radical. Therefore, upon approach of molecular oxygen to the [Fe^{III}(SPh)(cis-OTf)-(^{iPr}BIP)]^0 complex, during its binding to the vacant ligand position, the thiophenolate splits off as a SPh$^\cdot$ radical, Scheme 2. Collision of two thiophenyl radicals then will form PhS–SPh. Clearly, the binding affinity of molecular oxygen and the electron affinity of the complexes change from ligated triflate to chloride in the cis-position and as a consequence the complexes give differences in reactivity patterns.

An oxygen atom transfer reaction from complexes **A** or **B** to give sulfoxides or double oxygen atom transfer leads to sulfinic acid products. Both processes starting from iron(III)-superoxo will be initiated by breaking the dioxygen bond. In previous work, we showed that the hydrogen atom abstraction reaction by iron(IV)-oxo porphyrin cation radical oxidants is proportional to the strength of the C–H bond that is broken as well as with the O–H bond that is formed, i.e. the bond dissociation energy of the O–H bond or BDE$_{OH}$.[23b,26,37] On the other hand, in sulfoxidation reactions by metal–oxo oxidants it was shown that the O–S bond formation step is linearly proportional to the O–H bond
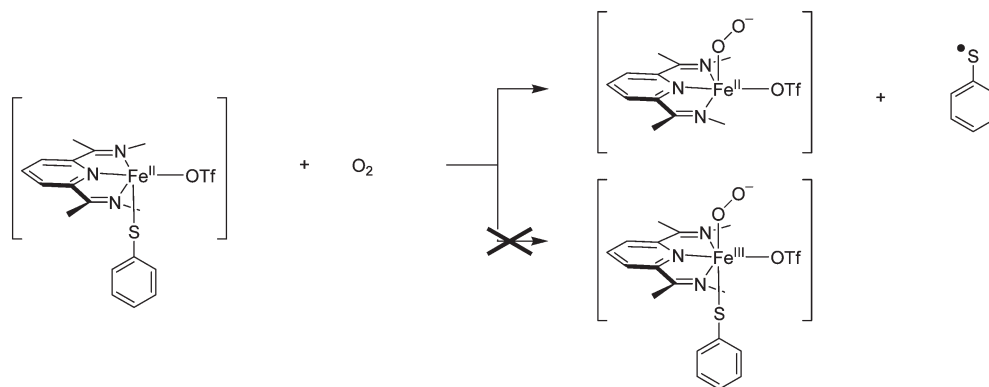
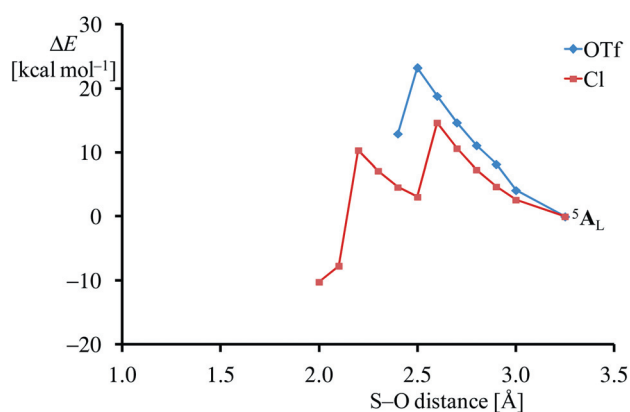**Scheme 2** Reaction of iron(II)-thiophenolate with dioxygen.

Fig. 6 Geometry scans for the attack of superoxo on the SPh⁻ group in $^5\mathbf{A_L}$ (L = Cl⁻ or OTf⁻). Each point in the figure represents a full geometry optimization (UB3LYP/B1) with fixed S–O distance in Gaussian. Energies are relative to $^5\mathbf{A_L}$ (L = Cl⁻ or OTf⁻).

r_{FeO} = 1.833 (2.009) [2.032]
$r_{\mathrm{FeS,cis}}$ = 2.427 (2.288) [2.350]
$r_{\mathrm{FeS,trans}}$ = 2.415 (2.422) [2.416]

$^1\mathbf{A_{SPh}}$ ($^3\mathbf{A_{SPh}}$) [$^5\mathbf{A_{SPh}}$]

r_{FeO} = 2.136 (2.121) [2.018]
$r_{\mathrm{FeCl,cis}}$ = 2.278 (2.288) [2.283]
$r_{\mathrm{FeCl,trans}}$ = 2.467 (2.464) [2.457]

$^1\mathbf{C_{Cl,Cl}}$ ($^3\mathbf{C_{Cl,Cl}}$) [$^5\mathbf{C_{Cl,Cl}}$]

Fig. 7 Optimized geometries of $^{1,3,5}\mathbf{A_{SPh}}$ (left-hand-side) and $^{1,3,5}\mathbf{C_{Cl,Cl}}$ (right-hand-side) with bond lengths in angstroms. Isopropyl groups have been hidden.

formation energy, and hence correlates with BDE$_{OH}$ as well.[37d,38] In a similar vein we predict complex $^5\mathbf{A_{Cl}}$ to be more efficient in oxygen atom transfer reactions to substrates since the superoxo bond is weaker, hence it should be easier to break in the process. To test this we ran a geometry scan for the attack of the terminal oxygen atom of the superoxo group on the sulfur atom of SPh⁻ for $^5\mathbf{A_{Cl}}$ and $^5\mathbf{A_{OTf}}$ and the results are given in Fig. 6. As follows, both reactions efficiently lead to a bicyclic ring structure, whereby an S–O bond is formed and the O–O bond is still intact, although weakened. This mechanism was also found for CDO enzymes using DFT and QM/MM methods.[8] Indeed, as predicted from the optimized geometries of $^5\mathbf{A_{Cl}}$ and $^5\mathbf{A_{OTf}}$, the barrier height for oxygen attack on sulfur is smaller for $^5\mathbf{A_{Cl}}$ than for $^5\mathbf{A_{OTf}}$.

How do our computations match the experiments reported on these particular systems? First of all, the crystal structure of Fe(II)-^{iPr}BIP with either chloride or triflate bound gave a structure of the **B**-type with chloride bound, but of **A**-type with triflate bound. These structures, of course, are pentacoordinated and no molecular oxygen is attached to the metal center. Nevertheless, we will compare the results obtained in this work with the pentacoordinate crystal structures from ref. 11. The relative energy between structures $^5\mathbf{A_{Cl}}$ and $^5\mathbf{B_{Cl}}$ is calculated to be 1.2 kcal mol⁻¹ in favour of structure **A**. Therefore both isomers

could exist in equilibrium in solution. On the other hand, for the triflate structure $^5\mathbf{A_{OTf}}$ is well lower in energy than $^5\mathbf{B_{OTf}}$ by 23 kcal mol⁻¹ due to the dissociation of the thiophenol from the metal center in **B**. It appears therefore that the cavity within the ^{iPr}BIP ligand is too small to fit the triflate ligand. On the other hand, small anions, such as chloride, fit into the cavity easily. As a consequence, the triflate bound structure resides in an orientation with the thiophenolate in the *cis*-position (equatorial), *i.e.* in a position adjacent to the superoxo group. Because of this positioning, the sulphur atom will be accessible for attack by dioxygen and efficient dioxygenation may occur. This result is indeed what Goldberg and co-workers observed with this complex. By contrast, the thiophenolate ligand is in the *trans*-position (axial) in the chloride bound structure, and it is located too far away from molecular oxygen to enable reactivity. However, these stable complexes may have a finite lifetime and during the course of that lifetime collisions of two $^5\mathbf{A_{Cl}}$ structures may occur that lead to disulfide product complexes.

To further ascertain the effect of *cis*-triflate on binding of thiophenolate in the *trans*-position, we calculated two additional structures, namely one with thiophenolate in both *cis* and *trans* positions ($\mathbf{A_{SPh}}$) and one with chloride in both *cis* and *trans* positions ($\mathbf{C_{Cl,Cl}}$), Fig. 7. Both structures, in analogy with $\mathbf{A_{Cl}}$, $\mathbf{A_{OTf}}$,

5406 | *Org. Biomol. Chem.*, 2012, **10**, 5401–5409

This journal is © The Royal Society of Chemistry 2012
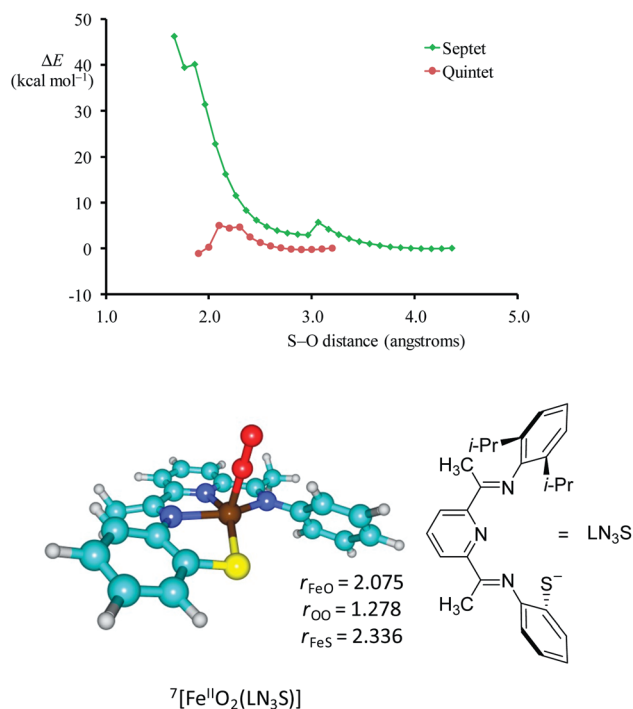
Fig. 8 Septet and quintet S–O bond formation scan and optimized geometry of $[FeO_2(LN_3S)]$ with distances in angstroms.

$\mathbf{B}_{Cl}$ and $\mathbf{B}_{OTf}$ discussed above have the quintet spin state well below the triplet and singlet spin states by more than 10 kcal mol^{-1}. Optimized geometries are in line with the structures displayed in Fig. 2 above with iron-*cis*-ligand distances of 2.350 and 2.283 Å for $^5\mathbf{A}_{SPh}$ and $^5\mathbf{C}_{Cl,Cl}$, respectively. The metal-*trans*-ligand distances are somewhat longer than the metal-*cis*-ligand ones, namely 2.416 and 2.457 Å for $^5\mathbf{A}_{SPh}$ and $^5\mathbf{C}_{Cl,Cl}$, respectively, which is a result of orbital occupation. Nevertheless, thiophenolate binds in the axial ligand position, but only when either chloride or thiophenolate is in the *cis*-position. Bulky triflate ligands, therefore, in the *cis*-position prevent binding of thiophenolate in the axial position and a dissociative system is found for $\mathbf{B}_{OTf}$.

In summary, the key feature that determines dioxygenation of thiophenol by these nonheme iron complexes appears to be the availability of a *cis*-binding site on the metal adjacent to the dioxygen binding position. Stereochemical interactions of ligands as in the case of structure **B** prevent binding of thiophenolate in an appropriate position and consequently cannot bind it. However, these complexes can donate electrons rather than binding substrate that will then lead to formation of PhS–SPh products.

How does the work compare to other computational studies of CDO model complexes? Recent computational studies[36] on a related CDO mimic with a bis(imino)pyridyl ligand and pendant thiolate group (LN_3S) revealed a sulphur dioxygenation mechanism similar to CDO enzymes on competing singlet, triplet and quintet spin state surfaces. In these studies the possible septet spin state was not considered. However, in light of recent experimental studies on CDO enzymes that seem to implicate a septet spin iron(III)-superoxo species,[29] as well as the studies

presented in this work, we decided to revisit our study and calculate the septet spin $[Fe^{II}O_2(LN_3S)]$ and its oxygen activation reaction.

As follows from Fig. 8 the iron(III)-superoxo structure in the septet spin state is slightly lower in energy to that found for the quintet spin state; in the gas-phase $\Delta E + ZPE$ is 1.8 kcal mol^{-1} whereas in solvent it is 0.9 kcal mol^{-1}. This implies that technically, the structure can exist in close lying septet and quintet spin state structures. To find out whether the septet spin state is reactive, we investigated the S–O bond formation step in the dioxygenation process of the LN_3S ligand. In the quintet spin state a low barrier of 5.0 kcal mol^{-1} was found. A geometry scan starting from the septet spin state (top panel in Fig. 8), however, shows a continuous climbing energy curve that does not reach a local minimum for an intermediate in the dioxygenation process. The maximum point of the scan is well higher in energy than reactants, *i.e.* by more than 40 kcal mol^{-1}. Clearly, the septet spin state, even if it exists, is an unreactive state that will not be able to participate in the reaction mechanism. Consequently, a spin crossing from septet back to quintet will be required for the dioxygenation process to proceed.

Conclusions

Density functional theory calculations are presented on biomimetic model complexes of cysteine dioxygenase. Our studies show that it is vital to have a thiolate substrate bound in the *cis*-position of the dioxygen moiety. Preventing substrate binding through stereochemical interactions of other ligands prevents substrate dioxygenation. However, the iron(III)-superoxo complex is a good electron acceptor and easily abstracts electrons from thiophenols so that they can react further to form PhS–SPh *via* a bimolecular reaction.

Acknowledgements

Notes and references

1 (*a*) E. I. Solomon, T. C. Brunold, M. I. Davis, J. N. Kemsley, S.-K. Lee, N. Lehnert, F. Neese, A. J. Skulan, Y.-S. Yang and J. Zhou, *Chem. Rev.*, 2000, **100**, 235; (*b*) T. D. H. Bugg, *Curr. Opin. Chem. Biol.*, 2001, **5**, 550; (*c*) M. Costas, M. P. Mehn, M. P. Jensen and L. Que Jr., *Chem. Rev.*, 2004, **104**, 939; (*d*) P. C. A. Bruijnincx, G. van Koten and R. J. M. Klein Gebbink, *Chem. Soc. Rev.*, 2008, **37**, 2716; (*e*) *Iron-Containing Enzymes: Versatile Catalysts of Hydroxylation Reactions in Nature*, ed. S. P. de Visser and D. Kumar, RSC Publishing, Cambridge (UK), 2011.
2 (*a*) C. Krebs, D. G. Fujimori, C. T. Walsh and J. M. Bollinger Jr, *Acc. Chem. Res.*, 2007, **40**, 484; (*b*) C. J. Schofield and Z. Zhang, *Curr. Opin. Chem. Biol.*, 1999, **9**, 722; (*c*) T. D. H. Bugg, *Tetrahedron*, 2003, **59**, 7075.

3 (*a*) O. W. Choroba, D. H. Williams and J. B. Spencer, *J. Am. Chem. Soc.*, 2000, **122**, 5389; (*b*) L. J. Higgins, F. Yan, P. Liu, H.-W. Liu and C. L. Drennan, *Nature*, 2005, **437**, 838; (*c*) M. J. Bodner, R. M. Phelan, M. F. Freeman, R. Li and C. A. Townsend, *J. Am. Chem. Soc.*, 2010, **132**, 12.

4 (*a*) S. C. Trewick, T. F. Henshaw, R. P. Hausinger, T. Lindahl and B. Sedgwick, *Nature*, 2002, **419**, 174; (*b*) P. Ø. Falnes, R. F. Johansen and E. Seeberg, *Nature*, 2002, **419**, 178; (*c*) Y. Mishina, E. M. Duguid and C. He, *Chem. Rev.*, 2006, **106**, 215.

5 (*a*) M. H. Stipanuk, *Annu. Rev. Nutr.*, 2004, **24**, 539; (*b*) G. D. Straganz and B. Nidetzky, *ChemBioChem*, 2006, **7**, 1536; (*c*) C. A. Joseph and M. J. Maroney, *Chem. Commun.*, 2007, 3338.

6 S. Ye, X. Wu, L. Wei, D. Tang, P. Sun, M. Bartlam and Z. Rao, *J. Biol. Chem.*, 2007, **282**, 3391.

7 (*a*) J. G. McCoy, L. J. Bailey, E. Bitto, C. A. Bingman, D. J. Aceti, B. G. Fox and G. N. Phillips Jr, *Proc. Natl. Acad. Sci. U. S. A.*, 2006, **103**, 3084; (*b*) S. C. Chai, J. R. Bruyere and M. J. Maroney, *J. Biol. Chem.*, 2006, **281**, 15774; (*c*) C. R. Simmons, Q. Liu, Q. Huang, Q. Hao, T. P. Begley, P. A. Karplus and M. H. Stipanuk, *J. Biol. Chem.*, 2006, **281**, 18723; (*d*) J. E. Dominy Jr, C. R. Simmons, P. A. Karplus, A. M. Gehring and M. H. Stipanuk, *J. Bacteriol.*, 2006, **188**, 5561; (*e*) B. D. Pierce, J. D. Gardner, L. J. Bailey, T. C. Brunold and B. G. Fox, *Biochemistry*, 2007, **46**, 8569; (*f*) J. E. Dominy Jr, J. Hwang, S. Guo, L. L. Hirschberger, S. Zhang and M. H. Stipanuk, *J. Biol. Chem.*, 2008, **283**, 12188; (*g*) T. Kleffmann, S. A. K. Jongkees, G. Fairweather, S. M. Wilbanks and G. N. L. Jameson, *J. Biol. Inorg. Chem.*, 2009, **14**, 913; (*h*) J. D. Gardner, B. S. Pierce, B. G. Fox and T. C. Brunold, *Biochemistry*, 2010, **49**, 6033; (*i*) E. P. Tchesnokov, S. M. Wilbanks and G. N. L. Jameson, *Biochemistry*, 2012, **51**, 257.

8 (*a*) S. Aluri and S. P. de Visser, *J. Am. Chem. Soc.*, 2007, **129**, 14846; (*b*) S. P. de Visser and G. D. Straganz, *J. Phys. Chem. A*, 2009, **113**, 1835; (*c*) D. Kumar, W. Thiel and S. P. de Visser, *J. Am. Chem. Soc.*, 2011, **133**, 3869.

9 (*a*) S. V. Kryatov, E. V. Rybak-Akimova and S. Schindler, *Chem. Rev.*, 2005, **105**, 2175; (*b*) M. M. Abu-Omar, A. Loaiza and N. Hontzeas, *Chem. Rev.*, 2005, **105**, 2227; (*c*) W. Nam, *Acc. Chem. Res.*, 2007, **40**, 522.

10 (*a*) Y. Jiang, L. R. Widger, G. D. Kasper, M. A. Siegler and D. P. Goldberg, *J. Am. Chem. Soc.*, 2010, **132**, 12214; (*b*) A. C. McQuilken, Y. Jiang, M. A. Siegler and D. P. Goldberg, *J. Am. Chem. Soc.*, 2012, **134**, 8758–8761.

11 Y. M. Badiei, M. A. Siegler and D. P. Goldberg, *J. Am. Chem. Soc.*, 2011, **133**, 1274.

12 M. Sallmann, I. Siewert, L. Fohlmeister, C. Limberg and C. Knispel, *Angew. Chem., Int. Ed.*, 2012, **51**, 2234.

13 (*a*) J. H. Dawson, R. H. Holm, J. R. Trudell, G. Barth, R. E. Linder, E. Bunnenberg, C. Djerassi and S. C. Tang, *J. Am. Chem. Soc.*, 1976, **98**, 3707; (*b*) T. L. Poulos, *J. Biol. Inorg. Chem.*, 1996, **1**, 356.

14 (*a*) M. T. Green, J. H. Dawson and H. B. Gray, *Science*, 2004, **304**, 1653; (*b*) W.-D. Woggon, *Acc. Chem. Res.*, 2005, **38**, 127.

15 D. Kumar, S. P. de Visser, P. K. Sharma, E. Derat and S. Shaik, *J. Biol. Inorg. Chem.*, 2005, **10**, 181.

16 F. Ogliaro, S. P. de Visser and S. Shaik, *J. Inorg. Biochem.*, 2002, **91**, 554.

17 (*a*) Z. Gross and S. Nimri, *Inorg. Chem.*, 1994, **33**, 1731; (*b*) Z. Gross, *J. Biol. Inorg. Chem.*, 1996, **1**, 368; (*c*) K. Czarnecki, S. Nimri, Z. Gross, L. M. Proniewicz and J. R. Kincaid, *J. Am. Chem. Soc.*, 1996, **118**, 2929.

18 (*a*) W. Nam, Y. O. Ryu and S. J. Song, *J. Biol. Inorg. Chem.*, 2004, **9**, 654; (*b*) W. J. Song, Y. O. Ryu, R. Song and W. Nam, *J. Biol. Inorg. Chem.*, 2005, **10**, 294.

19 (*a*) C. V. Sastri, J. Lee, K. Oh, Y. J. Lee, J. Lee, T. A. Jackson, K. Ray, H. Hirao, W. Shin, J. A. Halfen, J. Kim, L. Que Jr, S. Shaik and W. Nam, *Proc. Natl. Acad. Sci. U. S. A.*, 2007, **104**, 19181; (*b*) A. E. Anastasi, P. Comba, J. McGrady, A. Lienke and H. Rohwer, *Inorg. Chem.*, 2007, **46**, 6420; (*c*) M. P. Jensen, A. Mairata i Payeras, A. T. Fiedler, M. Costas, J. Kaizer, A. Stubna, E. Münck and L. Que Jr, *Inorg. Chem.*, 2007, **46**, 2398; (*d*) T. A. Jackson, J.-U. Rohde, M. S. Seo, C. V. Sastri, R. DeHont, A. Stubna, T. Ohta, T. Kitagawa, E. Münck, W. Nam and L. Que Jr, *J. Am. Chem. Soc.*, 2008, **130**, 12394; (*e*) Y. Zhou, X. Shan, R. Mas-Ballesté, M. R. Bukowski, A. Stubna, M. Chakrabarti, L. Slominski, J. A. Halfen, E. Münck and L. Que Jr, *Angew. Chem., Int. Ed.*, 2008, **47**, 1896; (*f*) H. Hirao, L. Que Jr, W. Nam and S. Shaik, *Chem.–Eur. J.*, 2008, **14**, 1740; (*g*) S. Fukuzumi, H. Kotani, T. Suenobu, S. Hong, J.-M. Lee and W. Nam, *Chem.–Eur. J.*, 2010, **16**, 354; (*h*) K.-B. Cho,

Y. Moreau, D. Kumar, D. A. Rock, J. P. Jones and S. Shaik, *Chem.–Eur. J.*, 2007, **13**, 4103.

20 (*a*) F. Namuswe, G. D. Kasper, A. A. N. Sarjeant, T. Hayashi, C. M. Krest, M. T. Green, P. Moënne-Loccoz and D. P. Goldberg, *J. Am. Chem. Soc.*, 2008, **130**, 14189; (*b*) J. Stasser, F. Namuswe, G. D. Kasper, Y. Jiang, C. M. Krest, M. T. Green, J. Penner-Hahn and D. P. Goldberg, *Inorg. Chem.*, 2010, **49**, 9178; (*c*) F. Namuswe, T. Hayashi, Y. Jiang, G. D. Kasper, A. A. N. Sarjeant, P. Moënne-Loccoz and D. P. Goldberg, *J. Am. Chem. Soc.*, 2010, **132**, 157.

21 (*a*) K. A. Prokop, S. P. de Visser and D. P. Goldberg, *Angew. Chem., Int. Ed.*, 2010, **49**, 5091; (*b*) K. A. Prokop, H. M. Neu, S. P. de Visser and D. P. Goldberg, *J. Am. Chem. Soc.*, 2011, **133**, 15874.

22 M. J. Frisch, G. W. Trucks, H. B. Schlegel, G. E. Scuseria, M. A. Robb, J. R. Cheeseman, J. A. Montgomery Jr, T. Vreven, K. N. Kudin, J. C. Burant, J. M. Millam, S. S. Iyengar, J. Tomasi, V. Barone, B. Mennucci, M. Cossi, G. Scalmani, N. Rega, A. Petersson, H. Nakatsuji, M. Hada, M. Ehara, K. Toyota, R. Fukuda, J. Hasegawa, M. Ishida, T. Nakajima, Y. Honda, O. Kitao, N. Nakai, M. Klene, X. Li, J. E. Knox, H. P. Hratchian, J. B. Cross, C. Adamo, J. Jaramillo, R. Gomperts, R. E. Stratmann, O. Yazyev, A. J. Austin, R. Cammi, C. Pomelli, J. W. Ochterski, P. Y. Ayala, K. Morokuma, G. A. Voth, P. Salvador, J. J. Dannenberg, V. G. Zakrzewski, S. Dapprich, A. D. Daniels, M. C. Strain, O. Farkas, D. K. Malick, A. D. Rabuck, K. Raghavachari, J. B. Foresman, J. V. Ortiz, Q. Cui, A. G. Baboul, S. Clifford, J. Cioslowski, B. B. Stefanov, G. Liu, A. Liashenko, P. Piskorz, I. Komaromi, R. L. Martin, D. J. Fox, T. Keith, M. A. Al–Laham, C. Y. Peng, A. Nanayakkara, M. Challacombe, P. M. W. Gill, B. Johnson, W. Chen, M. W. Wong, C. Gonzalez and J. A. Pople, *GAUSSIAN 03 (Revision C.02)*, Gaussian, Inc., Wallingford, CT, 2004.

23 (*a*) S. P. de Visser, *Chem.–Eur. J.*, 2006, **12**, 8168; (*b*) S. P. de Visser, *Angew. Chem., Int. Ed.*, 2006, **45**, 1790; (*c*) S. P. de Visser, *J. Am. Chem. Soc.*, 2006, **128**, 9813; (*d*) D. Kumar, B. Karamzadeh, G. N. Sastry and S. P. de Visser, *J. Am. Chem. Soc.*, 2010, **132**, 7656.

24 (*a*) A. D. Becke, *J. Chem. Phys.*, 1993, **98**, 5648; (*b*) C. Lee, W. Yang and R. G. Parr, *Phys. Rev. B*, 1988, **37**, 785.

25 P. J. Hay and W. R. Wadt, *J. Chem. Phys.*, 1985, **82**, 270.

26 S. P. de Visser, *J. Am. Chem. Soc.*, 2010, **132**, 1087.

27 T. Schwabe and S. Grimme, *Phys. Chem. Chem. Phys.*, 2007, **9**, 3397.

28 (*a*) D. Kumar, S. P. de Visser and S. Shaik, *Chem.–Eur. J.*, 2005, **11**, 2825; (*b*) S. P. de Visser, K. Oh, A.-R. Han and W. Nam, *Inorg. Chem.*, 2007, **46**, 4632; (*c*) A. K. Vardhaman, C. V. Sastri, D. Kumar and S. P. de Visser, *Chem. Commun.*, 2011, **47**, 11044.

29 J. A. Crawford, W. Li and B. S. Pierce, *Biochemistry*, 2011, **50**, 10241.

30 M. M. Mbughuni, M. Chakrabarti, J. A. Hayden, E. L. Bominaar, M. P. Hendrich, E. Münck and J. D. Lipscomb, *Proc. Natl. Acad. Sci. U. S. A.*, 2010, **107**, 16788.

31 (*a*) P. Rydberg, E. Sigfridsson and U. Ryde, *J. Biol. Inorg. Chem.*, 2004, **9**, 203; (*b*) K. P. Jensen, B. O. Roos and U. Ryde, *J. Inorg. Biochem.*, 2005, **99**, 45; (*c*) H. Nakashima, J.-Y. Hasegawa and H. Nakatsuji, *J. Comput. Chem.*, 2006, **27**, 1363; (*d*) J. Annaraj, J. Cho, Y.-M. Lee, S. Y. Kim, R. Latifi, S. P. de Visser and W. Nam, *Angew. Chem., Int. Ed.*, 2009, **48**, 4150; (*e*) S. P. de Visser, *Coord. Chem. Rev.*, 2009, **253**, 754; (*f*) W. Lai and S. Shaik, *J. Am. Chem. Soc.*, 2011, **133**, 5444; (*g*) R. Latifi, T. Tahsini, D. Kumar, G. N. Sastry, W. Nam and S. P. de Visser, *Chem. Commun.*, 2011, **47**, 10674; (*h*) K.-B. Cho, H. Chen, D. Janardanan, S. P. de Visser, S. Shaik and W. Nam, *Chem. Commun.*, 2012, **48**, 2189.

32 (*a*) S. P. de Visser, *J. Biol. Inorg. Chem.*, 2006, **11**, 168; (*b*) S. P. de Visser, L. Tahsini and W. Nam, *Chem.–Eur. J.*, 2009, **15**, 5577.

33 (*a*) J. P. Emerson, E. R. Farquhar and L. Que Jr, *Angew. Chem., Int. Ed.*, 2007, **46**, 8553; (*b*) W. A. van der Donk, K. Crebs and J. M. Bollinger Jr, *Curr. Opin. Struct. Biol.*, 2010, **20**, 1; (*c*) Y.-M. Lee, S. Hong, Y. Morimoto, W. Shin, S. Fukuzumi and W. Nam, *J. Am. Chem. Soc.*, 2010, **132**, 10668; (*d*) A. Mukherjee, M. A. Cranswick, M. Chakrabarti, T. K. Paine, K. Fujisawa, E. Münck and L. Que Jr, *Inorg. Chem.*, 2010, **49**, 3618.

34 (*a*) A. Bassan, T. Borowski and P. E. M. Siegbahn, *Dalton Trans.*, 2004, 3153; (*b*) S. Shaik, D. Kumar, S. P. de Visser, A. Altun and W. Thiel, *Chem. Rev.*, 2005, **105**, 2279; (*c*) V. Georgiev, T. Borowski, M. R. A. Blomberg and P. E. M. Siegbahn, *J. Biol. Inorg. Chem.*, 2008, **13**, 929; (*d*) L. T. Haahr, K. P. Jensen, J. Boesen and H. E. M. Christensen, *J. Inorg. Biochem.*, 2010, **104**, 136.

35 (*a*) S. P. de Visser, *J. Am. Chem. Soc.*, 2006, **128**, 15809; (*b*) L. Bernasconi and E. J. Baerends, *Eur. J. Inorg. Chem.*, 2008, 1672.

36 D. Kumar, G. N. Sastry, D. P. Goldberg and S. P. de Visser, *J. Phys. Chem. A*, 2012, **116**, 582.

37 (*a*) S. P. de Visser, D. Kumar, S. Cohen, R. Shacham and S. Shaik, *J. Am. Chem. Soc.*, 2004, **126**, 8362; (*b*) S. Shaik, D. Kumar and S. P. de Visser, *J. Am. Chem. Soc.*, 2008, **130**, 10128; (*c*) R. Latifi, M. Bagherzadeh and S. P. de Visser, *Chem.–Eur. J.*, 2009, **15**, 6651; (*d*) D. Kumar, G. N. Sastry and S. P. de Visser, *Chem.–Eur. J.*, 2011, **17**, 6196; (*e*) D. Kumar, G. N. Sastry and S. P. de Visser, *J. Phys. Chem. B*, 2012, **116**, 718; (*f*) R. Latifi, J. S. Valentine, W. Nam and S. P. de Visser, *Chem. Commun.*, 2012, **48**, 3491.

38 D. Kumar, S. P. de Visser, P. K. Sharma, H. Hirao and S. Shaik, *Biochemistry*, 2005, **44**, 8148.

This journal is © The Royal Society of Chemistry 2012

Org. Biomol. Chem., 2012, **10**, 5401–5409 | 5409